38. A. Bartolini *et al.*, *Geochem. Geophys. Geosyst.* **13**, Q01007 (2012).
39. A. von Hillebrandt, L. Krystyn, *Geologie und Palontologie* **253**, 163 (2009).
40. D. V. Kent, L. Tauxe, *Science* **307**, 240 (2005).

Acknowledgments: We express our gratitude to S. Burgess, N. Youbi, B. Schoene, J. Ramezani, D. Condon, and two anonymous reviewers. We acknowledge that this work owes much to the collective effort of the EARTHTIME community. We also thank Vulcan Materials and Carolina Sunrock LLC for quarry access, G. Fisher of the Alcatel-Lucent EH&S-Americas for Preakness Basalt cores, B. Smith for the Rossville and York Haven diabase samples, and J. Smoot and N. Ratcliff for access to cores and thin sections. We acknowledge support from the U.S. National Science Foundation (grants EAR-0446880 and EAR-0931839 to S.A.B., EAR 0753496 to P.E.O. and D.V.K., and EAR 0345664 to E.T.R.). P.E.O. received support from the Bahamas Petroleum Company. Data presented in this paper are fully documented in the supplementary materials. U-Pb zircon data are deposited at the Geochron database (www.geochron.org) with SESAR IGSNs SAB000002-SAB00000A, available at www.geochron.org/dataset/html/5QlSoX9SCtJbNfOZbNeXtuwSK.

Supplementary Materials
www.sciencemag.org/cgi/content/full/science.1234204/DC1
Materials and Methods
Supplementary Text
Figs. S1 to S5
Tables S1 to S3
References (*41*–*92*)

18 December 2012; accepted 28 February 2013
Published online 21 March 2013;
10.1126/science.1234204

Annually Resolved Ice Core Records of Tropical Climate Variability over the Past ~1800 Years

L. G. Thompson,[1,2]* E. Mosley-Thompson,[1,3] M. E. Davis,[1] V. S. Zagorodnov,[1] I. M. Howat,[1,2] V. N. Mikhalenko,[4] P.-N. Lin[1]

Ice cores from low latitudes can provide a wealth of unique information about past climate in the tropics, but they are difficult to recover and few exist. Here, we report annually resolved ice core records from the Quelccaya ice cap (5670 meters above sea level) in Peru that extend back ~1800 years and provide a high-resolution record of climate variability there. Oxygen isotopic ratios ($\delta^{18}O$) are linked to sea surface temperatures in the tropical eastern Pacific, whereas concentrations of ammonium and nitrate document the dominant role played by the migration of the Intertropical Convergence Zone in the region of the tropical Andes. Quelccaya continues to retreat and thin. Radiocarbon dates on wetland plants exposed along its retreating margins indicate that it has not been smaller for at least six millennia.

Ice cores from high-altitude tropical glaciers offer long-term perspectives on the variability of precipitation, temperature, aridity, and atmospheric and sea surface conditions at low latitudes. Most meteorological and climatic disturbances affecting Earth's surface and lower atmosphere originate in or are amplified by ocean-atmosphere interactions in tropical latitudes. As Earth's "heat engine," the warmest atmospheric and sea surface temperatures (SSTs) occur there. This energy drives intense convective precipitation and is crucial for the evolution of phenomena such as El Niño–Southern Oscillation (ENSO), the monsoonal systems of Asia and Africa, and, on intraannual time scales, hurricanes and other tropical disturbances that distribute equatorial heat energy poleward. ENSO dominates tropical climate variability. It is linked to the position of the Intertropical Convergence Zone (ITCZ), and its associated teleconnections affect the strength and direction of air masses and storm tracks, variations in convective activity that control flooding and drought, and modulation of tropical storm intensities. There are few high mountain glaciers in these regions and even fewer that preserve detailed histories of this variability. Unfortunately, most are now rapidly shrinking, and unique records are being lost. The potential impacts on water resources have social and economic consequences that underpin the imperative to understand the drivers and responses of past and present tropical climate variability.

The first ice cores drilled from the Quelccaya ice cap (QIC) [13°56′S, 70°50′W, 5670 m above sea level (masl)], in 1983 (*1*–*3*), could not be returned frozen to the laboratory and instead were cut into samples that were melted and bottled in the field. In 2003, two additional cores were drilled to bedrock on the QIC (Fig. 1). The Summit Dome (5670 masl) core (QSD, 168.68 m) and the North Dome (5600 masl) core (QND, 128.57 m) were returned frozen and are stored at –30°C at Ohio State University's Byrd Polar Research Center. Minimal postdepositional reworking of the snow surface, even during the wet season, results in the distinct annual layers (fig. S1A) used to reconstruct an ~1800-year climate history. Details about the construction of the time scale, extracting annually resolved information, and reconstructing the net annual accumulation are provided in the supplementary text. The oxygen isotopic ratio ($\delta^{18}O$) records for the 2003 QSD and QND cores, separated by 1.92 km, are highly correlated ($r = 0.898$, $P < 0.0001$ for decadal averages; table S1). In light of their similarity,

Fig. 1. Location of the QIC, Peru, and other ice fields and features discussed in the text. Also included are the upper (500 hPa) and lower (850 hPa) level atmospheric circulation in the austral summer [December-January-February (DJF)] (*38*).

[1]Byrd Polar Research Center, The Ohio State University, Columbus, OH 43210, USA. [2]School of Earth Sciences, The Ohio State University, Columbus, OH 43210, USA. [3]Department of Geography, The Ohio State University, Columbus, OH 43210, USA. [4]Institute of Geography, Russian Academy of Sciences, Moscow, Russia.

*Corresponding author. E-mail: thompson.3@osu.edu

documented in the supplementary text, all subsequent discussions are based on the QSD core.

These records (Fig. 2 and fig. S2), based on freshly cut ice samples, are precisely dated and include $\delta^{18}O$ and concentrations of insoluble dust and major anions (F^-, Cl^-, SO_4^{2-}, and NO_3^-) and cations (Na^+, NH_4^+, K^+, Mg^{2+}, and Ca^{2+}). The reproducibility of decadal averages of $\delta^{18}O$ (1983 Core 1 versus the 2003 QSD core) from 1000 to 1982 CE (fig. S3A) is excellent ($r = 0.856$, $P < 0.0001$). Details of the reproducibility of $\delta^{18}O$ and net accumulation among the four cores, two in 1983 and two in 2003, over the past 1000 years are in the supplementary text (fig. S3, A and B, and table S1).

The Record

Figure 2 presents the decadal averages of $\delta^{18}O$, net accumulation, insoluble dust, ammonium (NH_4^+), and nitrate (NO_3^-) measured in the QSD core. Decadal averages of all other species are shown in fig. S2. Because annual resolution is preserved to ~160 m (683 CE) (supplementary materials), the annual net accumulation (A_n) record terminates there. These histories detail changes in climatic and environmental conditions in the tropical Andes over the past 18 centuries.

Four distinct climatic stages are evident. Table S2 presents the average values of all QSD core constituents for the different time periods discussed in the paper. Before 1100 CE, most constituents show little variability, although accumulation and insoluble dust concentrations are slightly higher and decline slowly toward 1100 CE. Simultaneously, $\delta^{18}O$ becomes modestly depleted in ^{18}O.

The Medieval Climate Anomaly (MCA) is characterized by below-average A_n, consistent with hydroclimate reconstructions for this region (*4*), and $\delta^{18}O$ is more variable and modestly enriched [0.26 per mil (‰)] relative to the long-term average (–17.92‰) (table S2). MCA ice contains no visible evidence of surface melting or smoothing of the $\delta^{18}O$ annual signal that, as discussed below, characterizes the QIC core since 1991. For just 4 decades near the end of the MCA, the QSD core contains high levels of ammonium (NH_4^+) and nitrate (NO_3^-) that are not contemporaneous with $\delta^{18}O$ evidence of strong warming or any notable increase in A_n. During the MCA, the climate across South America appears highly variable, possibly reflecting the observed dipole in humidity over the northern and southern Amazon Basin (*5*). The result is that wetter conditions in the northeast tend to be contemporaneous with drier conditions in southern Amazonia. For example, a high-resolution record of El Niño flooding from a marine core off the coast of Peru at 12°S indicates intense aridity from 800 to 1250 CE (*6*), whereas the Cariaco Basin (Venezuela) titanium record (*7*) reflects wetter-than-average conditions in the northeast Amazon Basin from 950 to 1450 CE.

The most prominent feature in the QIC record is the Little Ice Age (LIA). Early in the 16th century, concentrations of ammonium, nitrate, calcium, magnesium, and sulfate began to increase (Fig. 2, fig. S2, and table S2). The period from ~1520 to 1880, identified as the LIA, is characterized by lower $\delta^{18}O$ values that remained low until the late 19th century. The net accumulation trend is distinctive. In ~1520 CE, A_n increased rapidly but declined abruptly in ~1680 CE from record highs in the Early LIA (1520 to 1680 CE) to record lows (~1800 CE) in the Late LIA (1681 to 1880 CE). Over much of the LIA, concentrations of most ionic species were persistently high but declined rapidly near the end as A_n began to increase.

With the onset of the Current Warm Period (CWP, 1880 CE to the present), both $\delta^{18}O$ and A_n increased, whereas all aerosol concentrations have remained low over much of the CWP. Over the past 30 years, most aerosol concentrations have increased severalfold primarily because of postdepositional surface melting and percolation through the firn pack. The firn-ice transition is at 17.7 m and corresponds to 1992; however, isotopic smoothing in the top of the record indicates that, since the onset of the melting and retreat of the ice cap in ~1991, meltwater has percolated down to the 1980 level [see figure 4 in (*8*)].

Linkages with the Tropical Pacific

The seasonal temperature range in the tropics is only a few degrees, whereas the seasonal differences in the $\delta^{18}O$ of Andean snowfall are much larger, often up to 20‰. Because 70 to 80% of the precipitation falling on Quelccaya arrives during the wet season, the $\delta^{18}O$ history reflects primarily conditions during austral summer. Decadal averages of precipitation amount and $\delta^{18}O$ are not strongly related (fig. S3). Twenty-one-year running correlations between $\delta^{18}O$ and A_n alternate between positive and negative values over multiple decades (fig. S4), and very few coefficients are significant at the 95% level. Essentially, there is no consistent, long-term statistically significant relationship between the amount of precipitation and its $\delta^{18}O$ signature. In general, low-latitude isotopic ratios yield a climate signal reflecting a variety of hydrologic and thermal influences in the broad geographic region that supplies moisture to the high glaciated mountains (*9*).

Although the moisture source for Quelccaya precipitation is primarily from the tropical Atlantic via the Amazon Basin, Vuille *et al.* (*10*) demonstrated that Pacific SSTs exert the dominant control on interannual $\delta^{18}O$ variability preserved in tropical Andean ice cores. This occurs via the expansion of the tropical troposphere associated with a warm tropical Pacific and enhanced westerly flow over the tropical Andes or via the shrinkage of the tropical troposphere associated with a cool tropical Pacific, and enhanced easterly flow over the subtropical Andes. These upper-level wind anomalies force the low-level moisture flow over the Andes and thereby link oceanic forcing and climate variability on interannual time scales.

Bradley *et al.* (*11*) demonstrated that $\delta^{18}O$ in the Sajama (Bolivia) ice core is more closely linked to SSTs, and hence to ENSO variability, across the equatorial Pacific Ocean even though the moisture source for precipitation is the Atlantic. A $\delta^{18}O$ composite of three Peruvian ice cores and one Himalayan ice core from 1856 to 1996 CE [see figure 3 in (*8*)] is strongly linked ($r = 0.73$; $P < 0.0001$, for 5-year moving averages) to the NINO4 extended reconstructed SSTs [ERSST (*12*)]. This strong relationship between ice core isotopic records throughout the tropics and tropical SSTs likely reflects the dominance of tropical evaporation in determining water vapor flux into the atmosphere (*13*). This also provides a

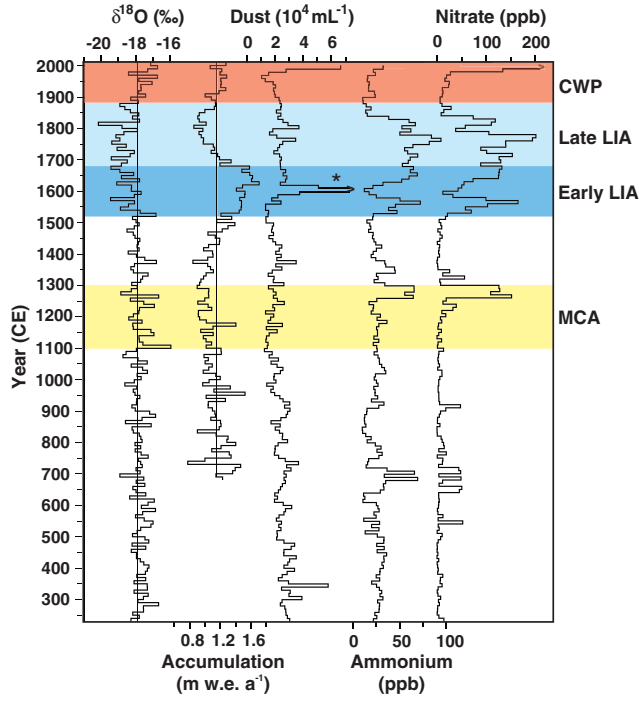

Fig. 2. Decadal averages of $\delta^{18}O$, net accumulation, insoluble dust, ammonium, and nitrate in the QSD ice core. Specific climatological periods discussed in the text are shaded and identified. The asterisk on the dust profile indicates the 1600 CE eruption of Huaynaputina (Peru). ppb indicates parts per billion; m w.e. a^{-1} indicates meters of water equivalent per year.

likely explanation of the large-scale isotopic links among low-latitude, high-altitude ice core records (*14*).

Figure 3A illustrates the spatial distribution of the correlations between the annual QSD $\delta^{18}O$ and ERSST records between 80°N and 80°S from 1870 to 2009 CE (*15*, *16*). The 2003 ice core record was extended to 2009 by using subsequently collected pit and shallow core samples. The annual $\delta^{18}O$ values of QIC precipitation are positively related to equatorial SSTs in the mid to eastern tropical Pacific Basin (solid line encloses $P < 0.001$). Correlations between the thermal-year (July to June) averages of $\delta^{18}O$ in the QSD core and ERSSTs in the NINO4, NINO3.4, and NINO3 regions were examined. The NINO4 SSTs are most strongly related to the QSD $\delta^{18}O$ ($r = 0.55$ for annual data; $r = 0.61$ for 3-year averages; $P < 0.0001$).

Figure 3B shows the 3-year running means of the NINO4 SST index (*12*) and QSD $\delta^{18}O$ for thermal years 1870-1871 to 2009-2010. Given their strong correlation ($r = 0.61$, $P < 0.0001$; fig. S5), the resulting SST-$\delta^{18}O$ transfer function ($SST_{NINO4} = 0.19 \times \delta^{18}O + 29.64$) is used to reconstruct a contemporaneous SST history for the NINO4 region (Fig. 3C) for the past 18 centuries. The reconstructed SSTs range between 25.8° and 26.6°C (decadal averages) or 25.0° to 27.1°C (annual data) with temperatures in the region depressed by 0.2°C during the LIA (1520 to 1880 CE) relative to the 20th-century average.

This reconstruction assumes that the QSD $\delta^{18}O$–NINO4 SST relationship has been stationary over the past 1800 years, which is not the nature of climate processes. The spatial distribution of the most highly correlated fields is not stationary through time (fig. S6). From near the end of the LIA (1870 CE) to 1900 CE, the enriched values of QSD $\delta^{18}O$ are strongly related to higher SSTs in the eastern Pacific region along the equator and extending southward. Note the strong positive correlation in the equatorial Atlantic at this time as well. Over the next 50 years (1901 to 1950 CE), the $\delta^{18}O$-SST correlations weaken, and the region of strongest positive correlations moves northward. In the past ~60 years (1951 to 2009 CE) during which anthropogenic forcing has increased (*17*), the region of strongest correlation increases in coherence and migrates north of the equator. The movement of the fields of significant $\delta^{18}O$-SST correlation into the Northern Hemisphere over the CWP likely reflects the post-LIA northward migration of the ITCZ over the tropical Pacific Basin, consistent with other evidence, including lake sediments from central equatorial Pacific islands (*18*).

A comprehensive review of various proxy indicators from diverse tropical sites (*19*) suggests a widespread southward migration of the ITCZ over the Holocene (their figure 12-5) affecting the Pacific, Indian, and Atlantic basins. In general, wetter conditions in the northern tropics gave way to more arid conditions in the late Holocene, whereas the southern tropics experienced the reverse trend. This plus evidence from coral records from the tropical Pacific (*20*) indicate that the movement of the ITCZ was coherent between the Atlantic and Pacific oceans (*19*). The climatological controls on snow accumulation and the isotopic chemistry of precipitation on the QIC are likely to change with the position of the ITCZ. Thus, the QSD records should provide additional details of the ITCZ migration.

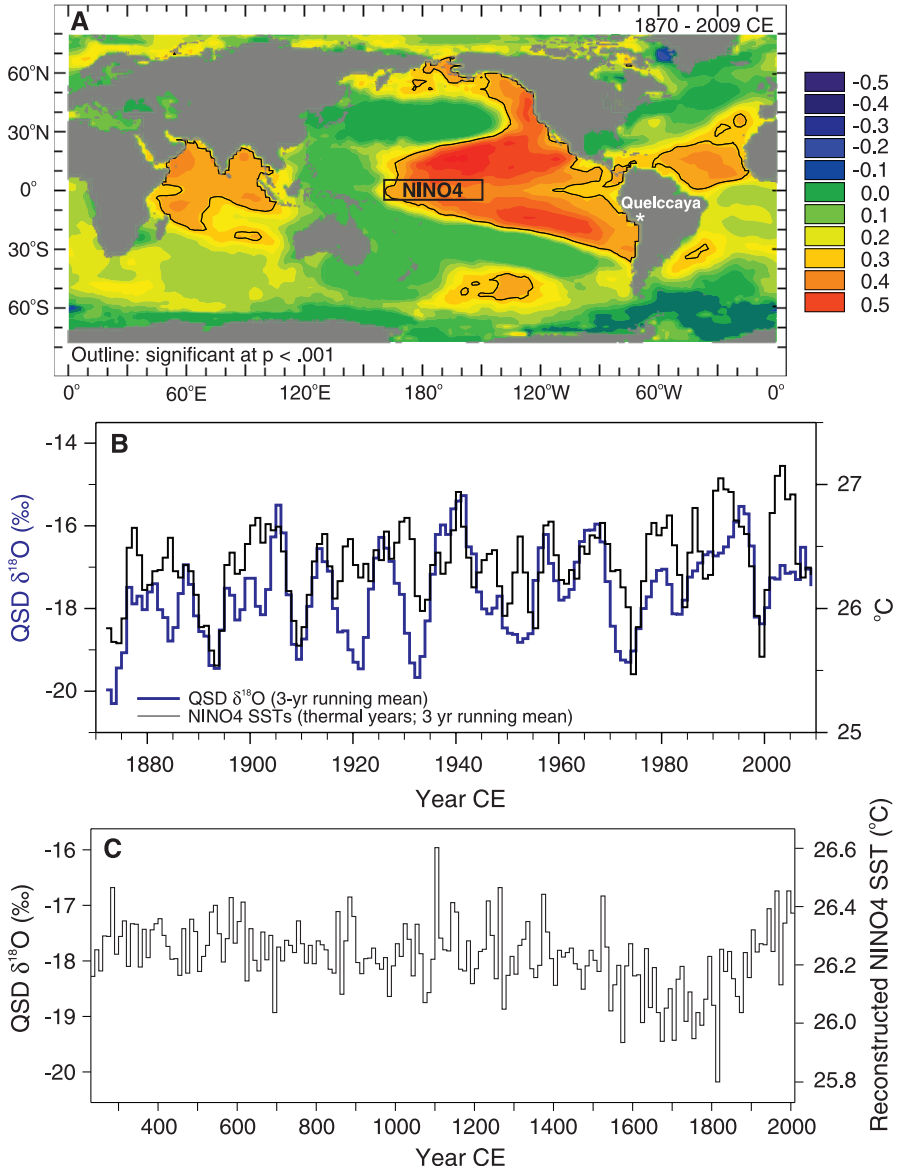

Fig. 3. QSD $\delta^{18}O$ and SST comparisons. (**A**) Spatial distribution of correlations between the annual QSD $\delta^{18}O$ and ERSST records [(*15*, *16*) and http://iridl.ldeo.columbia.edu/SOURCES/.NOAA/.NCDC/.ERSST/.version3b/.sst/] between 30°N and 30°S from 1870 to 2009 CE. (**B**) Three-year running means of the thermal-year averages of QSD $\delta^{18}O$ and SSTs in the NINO4 region [(*12*) and www.esrl.noaa.gov/psd/gcos_wgsp/Timeseries/Nino4] from 1871 to 2009 CE. (**C**) ~1800 year SST history reconstructed by using the QSD $\delta^{18}O$/SST regression equation (fig. S5) for data in (B).

ITCZ Migration and Tropical Linkages

As discussed above, the tropical eastern Pacific SSTs and atmospheric circulation influence the stable isotopic composition of the precipitation falling on Quelccaya, as well as on other central Andean glaciers (*11*, *21*). However, much of the precipitation falling on the eastern side of the Peruvian Andes is produced by deep convection in the tropical Amazon Basin during the austral summer. Much of the water vapor originates in the tropical Atlantic, as it has since the Last Glacial Maximum. This is confirmed by mountain snow lines that were tilted toward the Amazon Basin then as they are now (*22*).

Elevated concentrations of nitrate (NO_3^-) and ammonium (NH_4^+) and ^{18}O depleted isotopes in the QSD during the LIA are contemporaneous with decreasing percentages of Ti in the Cariaco Basin record off the coast of Venezuela at 10°N (Fig. 4). Reduced Ti concentrations indicate

decreased precipitation and runoff from the northeast coast of tropical South America (*7*). Conversely, elevated NO_3^- and NH_4^+ likely reflect more moist conditions to the south over the Amazon Basin. These aerosol species originate in part as products from ammonia (NH_3), a gas produced by biological activity in the soil and vegetation in the Amazon Basin (*23*, *24*). NO_3^- and NH_4^+ are correlated over the entire QSD core ($r = 0.76$, $P < 0.0001$ for decadal averages, from 230 to 1990 CE) and covary most strongly ($r = 0.92$, $P < 0.0001$) over the LIA. QSD NH_4^+ and therefore NO_3^- concentrations are significantly correlated with precipitable water in the southwest Amazon Basin from 1949 to 2002 (Fig. 5).

Both the Cariaco Basin and the Caribbean Sea lie along the path of moisture flow to the central Andes and experienced lower SSTs during the LIA (*25*, *26*). The Quelccaya $\delta^{18}O$ values also suggest lower SSTs in the tropical Pacific (Fig. 3C) at this time, indicating a LIA cooling in both ocean basins. Hydrological conditions were more regionally variable, and the QSD records suggest more complex large-scale linkages, possibly reflecting the recent northward migration of the ITCZ. However, over the Amazon Basin the ITCZ is not well defined but appears as a wide area of continental convection that is connected with the convergence zones over both the tropical Pacific and Atlantic oceans. Thus, its migration is not a simple shift into subtropical latitudes (*27*), and the associated precipitation anomalies are more complex. For example, lake (*28*) and speleothem (*29*) records in northern Peru indicate wet conditions, whereas speleothem records in northeastern Brazil (*30*) suggest dry conditions during the LIA.

Water levels measured in Lake Titicaca show reasonable similarities with the Quelccaya composite A_n before 1975 (fig. S7). Thereafter, mass wasting on the QIC has led to decreasing net accumulation. Marengo (*5*) demonstrated that even under current warmer conditions precipitation cycles in the northern and southern Brazilian Amazon Basin are out of phase, with both showing precipitation trend reversals in the mid-1940s and 1970s. Both QSD A_n and Lake Titicaca water level records closely reflect the timing and magnitude of changes in the Northern Amazonia Rainfall Index from 1929 to 1998 [figure 3 in (*5*)], which the author links to changes in oceanic and atmospheric circulation patterns and SSTs in the tropical central and eastern Pacific. These patterns argue not only that the QSD A_n represents the larger-scale regional pattern in Amazonian precipitation but that the NO_3^- and NH_4^+ signals likely originate in the Amazon Basin northeast of the QIC (Fig. 5) as a result of northeast airflow at the 850-mbar level (Fig. 1). Figure 4 illustrates that over the past ~1800 years the LIA is the most prominent feature in three ice-core records (Huascarán, Quelccaya, and Illimani; Fig. 1) collected along a north-to-south Andean transect. The relationships among these records suggest large-scale regional climate variability that requires multiple ice cores to disentangle the complex atmospheric and hydrological dynamics of the region.

The QIC accumulation history represents a much larger regional signal of precipitation variability. A_n on Quelccaya (Fig. 2) was well above average in the first half of the LIA (1520 to 1680 CE) and much reduced during the second half (1680 to 1880 CE). The A_n record is very similar to the 400-year climate history based on pollen (Poaceae/Asteraceae or P/A ratios) from the Sajama ice cap (Bolivia) 350 km to the southwest (*31*) and is consistent with nearby records of LIA glacier advance (*32*). The highest A_n rate in the QSD record is contemporaneous with the maximum LIA glacial extent (1630 to 1680 CE) in Bolivia and Peru, suggesting a cool and humid period followed by drier and gradually warming conditions as glaciers retreated. The humidity of the Bolivian/Peruvian Altiplano is reflected over long time scales by the nearby Lake Titicaca record (*33*).

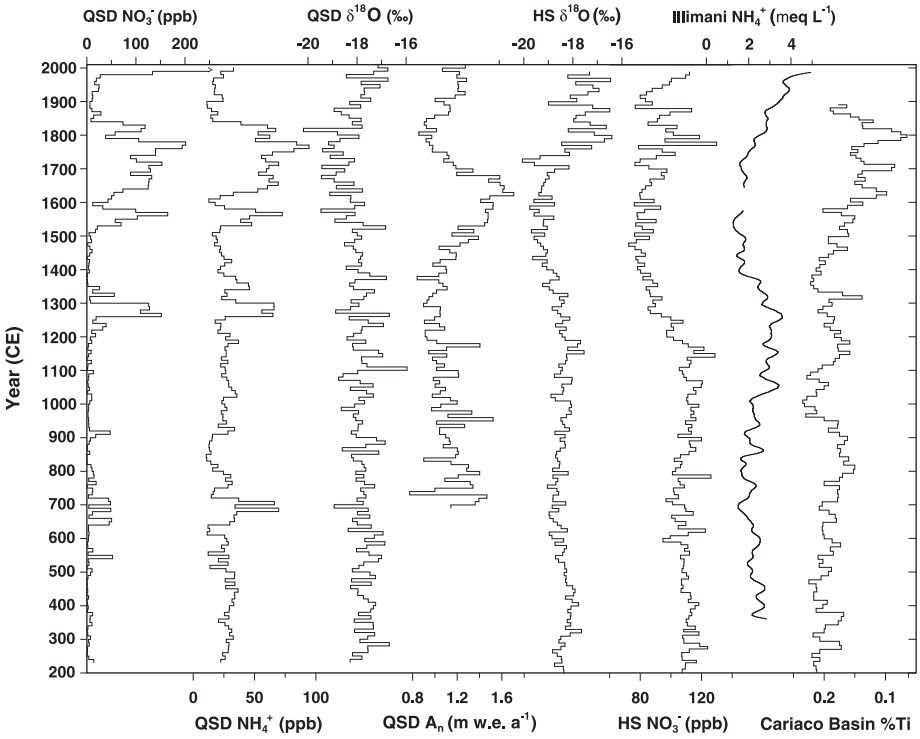

Fig. 4. Decadal averages of nitrate, ammonium, $\delta^{18}O$, net accumulation from QIC's QSD, $\delta^{18}O$ and nitrate from Huascarán in northern Peru (*34*), and Ti from Cariaco Basin (*7*). Note reversed axis for Ti. Illimani ice cap ammonium data are courtesy of M. Schwikowski (Paul Scherrer Institut).

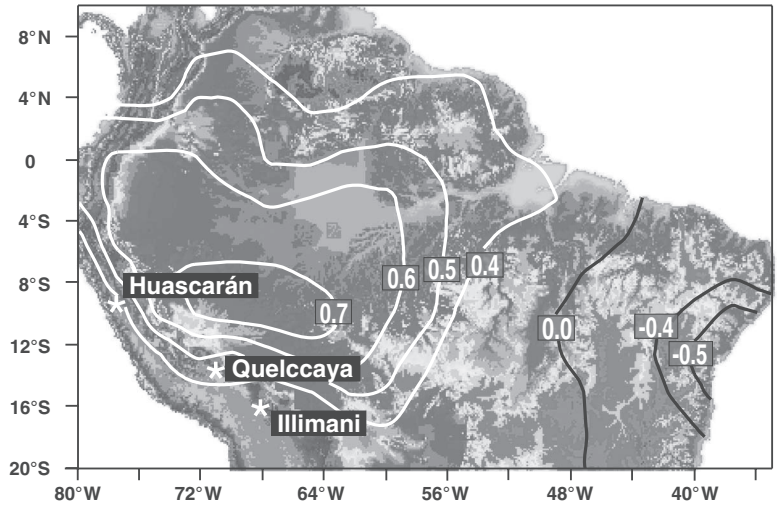

Fig. 5. Correlation fields between National Centers for Environmental Prediction/National Center for Atmospheric Research summertime (December to February) precipitable water (*39*) and annual ammonium concentrations from 1949 to 2002 in the QSD.

Thus, the QSD A_n record reflects larger regional changes in precipitation and indicates that Lake Titicaca's water level was likely above average from ~1520 to ~1680, after which it declined to much lower levels until rising again in the 20th century.

Throughout the LIA, elevated concentrations of NO_3^- and NH_4^+ on Quelccaya are contemporaneous with reduced Ti deposition in the Cariaco Basin (*7*) (Fig. 4), which indicates arid conditions in the northeast portion of the Amazon Basin. If the relationship between precipitable water and QSD NH_4^+ and NO_3^- (Fig. 5) persisted over the LIA, then wetter conditions in the southwest Amazon Basin just upwind of Quelccaya would be contemporaneous with drier conditions in northeast Brazil (*30*), consistent with a southward migration of the ITCZ (fig. S6), resulting in a region of intense continental convection over tropical Amazon Basin. Strong similarities exist between the oxygen isotope records from Quelccaya and Huascarán to the north; however, the differences between the QSD NH_4^+ record and the Huascarán NO_3^- (*34*) and Illimani NH_4^+ (*24*) records tell a different story (Fig. 5), suggesting different sources for these species.

The QIC NO_3^- and NH_4^- concentrations reflect hydrological conditions in the Amazon Basin northeast of Quelccaya (Fig. 5) with moisture advected to the site by northeasterly winds at the 850 hPa level (Fig. 1) (below the boundary layer). However, the moisture bringing the $\delta^{18}O$, the NO_3^- deposited on Huascarán (6050 masl), and the NH_4^+ deposited on Illimani (6300 masl) arrives via winds at the 500-hPa level originating from the east-southeast. Because both Illimani and Huascarán are located outside the area where QSD and NH_4^+ are correlated with precipitable water (Fig. 5), this points to the complexity of precipitation and chemistry patterns in the Andes. Additional linkages are discussed in the supplementary text, but, whatever the ultimate driver, NH_4^+ cannot be interpreted as a large-scale regional temperature recorder in all tropical ice cores.

Modern Retreat of the Margin of the Quelccaya Ice Cap

Nearly annual field observations confirm that since 1978 the QIC has been retreating along its margins (*14*). Radiocarbon-dated wetland plants exposed by the retreating ice provide temporal constraints on both its advance and retreat. Twenty wetland plants exposed by the retreating margin of the QIC were collected between 2004 and 2007 next to a meltwater lake (site A in Fig. 6) that started forming in 1985 on the west side of the ice cap. Radiocarbon dates for the plants [4676 ± 41 years before the present (yr B.P.)] indicate that the ice cap is smaller than it has been in almost five millennia (*14*, *35*). In 2011 as the ice cap continued to retreat, fresh plant remains were uncovered on the eastern side of the expanding North Lake (site B in Fig. 6), while most of the plants exposed in 2002 had already decayed because of their lack of woody tissue. Radiocarbon dates on these newly exposed plants, still in growth position, average 6298 ± 35 yr B.P. (table S3), ~1600 years older than the plants collected on the west side of the lake, indicating that Quelccaya is now smaller than it was 6000 years ago. Moreover, the plant ages confirm that the advance of the QIC ~6000 years ago was much slower, ~300 m over ~1600 years, than its current rate of retreat, ~300 m in 25 years. $\delta^{18}O$ is not correlated with net accumulation on decadal and longer time scales (Fig. 2 and figs. S3 and S4) but is highly correlated with SSTs in the eastern equatorial Pacific (Fig. 3, A and B). For the past century, Quelccaya's net accumulation has been above average, while $\delta^{18}O$ has been enriched (Fig. 2), suggesting that the current retreat is driven in part by its warming environment. The rapidity of Quelccaya's retreat may reflect snow-ice feedbacks that are considered instrumental (*36*) for rapidly increasing temperature trends near the 0°C isotherm during the 20th century. The accelerating retreat of Quelccaya and other tropical ice fields (*8*) is consistent with model predictions for vertical amplification of temperature in the tropics (*37*) and has serious implications for those living in these areas.

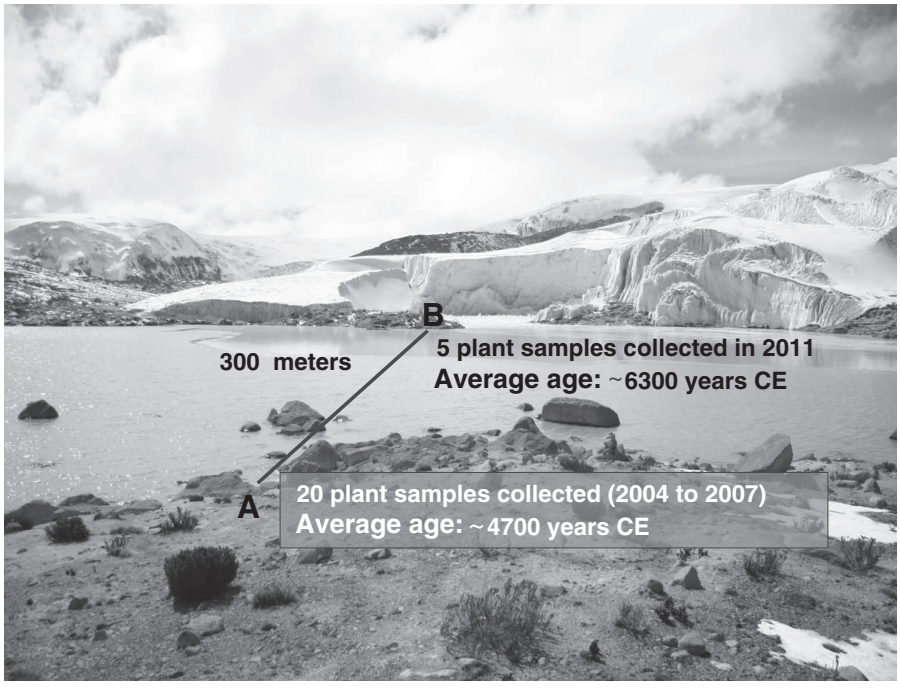

Fig. 6. Locations of recently exposed plants collected along the western side of the QIC.

References and Notes

1. L. G. Thompson, E. Mosley-Thompson, J. F. Bolzan, B. R. Koci, *Science* **229**, 971 (1985).
2. L. G. Thompson, E. Mosley-Thompson, W. Dansgaard, P. M. Grootes, *Science* **234**, 361 (1986).
3. L. G. Thompson, M. E. Davis, E. Mosley-Thompson, K.-B. Liu, *Nature* **336**, 763 (1988).
4. H. F. Diaz *et al.*, *Bull. Am. Meteorol. Soc.* **92**, 1487 (2011).
5. J. A. Marengo, *Theor. Appl. Climatol.* **78**, 79 (2004).
6. B. Rein, A. Lückge, F. Sirocko, *Geophys. Res. Lett.* **31**, L17211 (2004).
7. G. H. Haug, K. A. Hughen, D. M. Sigman, L. C. Peterson, U. Röhl, *Science* **293**, 1304 (2001).
8. L. G. Thompson, E. Mosley-Thompson, M. E. Davis, H. H. Brecher, *Ann. Glaciol.* **52**, 23 (2011).
9. M. Vuille, R. S. Bradley, M. Werner, R. Healy, F. Keimig, *J. Geophys. Res.* **108**, 4174 (2003).
10. M. Vuille *et al.*, *J. Geophys. Res.* **108**, 4175 (2003).
11. R. S. Bradley, M. Vuille, D. Hardy, L. G. Thompson, *Geophys. Res. Lett.* **30**, 1174 (2003).
12. N. A. Rayner *et al.*, *J. Geophys. Res.* **108**, 4407 (2003).
13. E. A. Boyle, *Geophys. Res. Lett.* **24**, 273 (1997).
14. L. G. Thompson *et al.*, *Proc. Natl. Acad. Sci. U.S.A.* **103**, 10536 (2006).
15. Y. Xue, T. M. Smith, R. W. Reynolds, *J. Clim.* **16**, 1601 (2003).
16. T. M. Smith, R. W. Reynolds, T. C. Peterson, J. Lawrimore, *J. Clim.* **21**, 2283 (2008).
17. IPCC, *Climate Change 2007: The Physical Science Basis: Contribution of Working Group I to the Fourth Assessment Report of the Intergovernmental Panel on Climate Change*, S. Solomon *et al.*, Eds. (Cambridge Univ. Press, New York, 2007).
18. J. P. Sachs *et al.*, *Nat. Geosci.* **2**, 519 (2009).
19. A. Koutavas, J. Lynch-Stieglitz, in *The Hadley Circulation: Past, Present and Future*, H. F. Diaz, R. S. Bradley, Eds., vol. 21 of *Advances in Global Change Research* (Kluwer Academic, Boston, 2004), pp. 347–369.
20. R. B. Dunbar, B. K. Linsley, G. M. Wellington, in *Climatic Variations and Forcing Mechanisms of the Last 2000 Years*, P. D. Jones, R. S. Bradley, J. Jouzel, Eds. (Springer-Verlag, Berlin, 1996), pp. 375–407.
21. K. A. Henderson, L. G. Thompson, P.-N. Lin, *J. Geophys. Res.* **104**, 31,053 (1999).
22. A. G. Klein, B. L. Isacks, A. L. Bloom, *Bull. Inst. Fr. Etudes Andines* **24**, 607 (1995).
23. G. P. Robertson, J. M. Tiedje, *Nature* **336**, 757 (1998).
24. T. Kellerhals *et al.*, *J. Geophys. Res.* **115**, D16123 (2010).
25. D. E. Black *et al.*, *Paleoceanography* **22**, PA4204 (2007).
26. A. Haase-Schramm *et al.*, *Paleoceanography* **18**, 1073 (2003).
27. R. Garreaud, M. Vuille, A. C. Clement, *Palaeogeogr. Palaeoclimatol. Palaeoecol.* **194**, 5 (2003).
28. B. W. Bird *et al.*, *Proc. Natl. Acad. Sci. U.S.A.* **108**, 8583 (2011).
29. J. Reuter *et al.*, *Geophys. Res. Lett.* **36**, L21706 (2009).
30. V. F. Novello *et al.*, *Geophys. Res. Lett.* **39**, L23706 (2012).
31. K.-B. Liu, C. A. Reese, L. G. Thompson, *Quat. Res.* **64**, 272 (2005).
32. V. Jomelli *et al.*, *Palaeogeogr. Palaeoclimatol. Palaeoecol.* **281**, 269 (2009).
33. P. A. Baker *et al.*, *Science* **291**, 640 (2001).

34. L. G. Thompson *et al.*, *Science* **269**, 46 (1995).
35. A. M. Buffen, L. G. Thompson, E. Mosley-Thompson, K. I. Huh, *Quat. Res.* **72**, 157 (2009).
36. N. C. Pepin, J. D. Lundquist, *Geophys. Res. Lett.* **35**, L14701 (2008).
37. R. S. Bradley, F. T. Keimig, H. F. Diaz, D. R. Hardy, *Geophys. Res. Lett.* **36**, L17701 (2009).
38. M. Vuille, *Int. J. Climatol.* **19**, 1579 (1999).
39. E. Kalnay *et al.*, *Bull. Am. Meteorol. Soc.* **77**, 437 (1996).

Acknowledgments: Funding was provided by NSF Paleoclimate Program award ATM-0318430 and the Ohio State University's Climate, Water and Carbon Program. We thank all the field and laboratory team members, many from the Byrd Polar Research Center, who have worked so diligently over the years to acquire these ice cores and extract their preserved climate histories. We acknowledge the efforts of our Peruvian colleagues from the Servicio Nacional de Meteorologia e Hidrologia, C. Portocarrero, and our mountaineers, led by B. Vicencio, who cooperated with us to make the project possible. Accelerator mass spectrometry ^{14}C measurements were made at the National Ocean Sciences Accelerator Mass Spectrometry Facility (Woods Hole Oceanographic Institution). This is Byrd Polar Research Center Contribution Number 1430. The data are archived at the National Oceanic and Atmospheric Administration World Data Center-A for Paleoclimatology: ftp://ftp.ncdc.noaa.gov/pub/data/paleo/icecore/trop/quelccaya/quelccaya2013.txt.

Supplementary Materials
www.sciencemag.org/cgi/content/full/science.1234210/DC1
Materials and Methods
Figs. S1 to S6
Tables S1 to S3
References (*40*–*42*)

18 December 2012; accepted 21 March 2013
Published online 4 April 2013;
10.1126/science.1234210

REPORTS

An Accurate Geometric Distance to the Compact Binary SS Cygni Vindicates Accretion Disc Theory

J. C. A. Miller-Jones,[1]* G. R. Sivakoff,[2,3] C. Knigge,[4] E. G. Körding,[5] M. Templeton,[6] E. O. Waagen[6]

Dwarf novae are white dwarfs accreting matter from a nearby red dwarf companion. Their regular outbursts are explained by a thermal-viscous instability in the accretion disc, described by the disc instability model that has since been successfully extended to other accreting systems. However, the prototypical dwarf nova, SS Cygni, presents a major challenge to our understanding of accretion disc theory. At the distance of 159 ± 12 parsecs measured by the Hubble Space Telescope, it is too luminous to be undergoing the observed regular outbursts. Using very long baseline interferometric radio observations, we report an accurate, model-independent distance to SS Cygni that places the source substantially closer at 114 ± 2 parsecs. This reconciles the source behavior with our understanding of accretion disc theory in accreting compact objects.

The accretion of matter onto a central compact object via a disc powers systems as diverse as active galactic nuclei (AGN), x-ray binaries (XRBs), cataclysmic variables (CVs), and young stellar objects. This universal process directly impacts the surrounding environment by driving powerful outflows and jets. CVs, which comprise a white dwarf accreting via Roche lobe overflow from a low-mass stellar companion, provide excellent laboratories for studying disc accretion. There is a large population of nearby CVs, and during outburst the accretion disc both dominates the observed emission at all wavelengths and exhibits structural changes on accessible time scales.

When the mass transfer rate through an accretion disc is sufficiently high, the disc will remain in a fully ionized, stable state. At lower accretion rates, the resulting lower temperatures allow the recombination of hydrogen, leading to large changes in the disc opacity. This alters the disc cooling mechanism and causes the disc to become thermally unstable, leading to the semi-regular outburst events seen in dwarf nova CVs. The disc instability model (DIM) describes the resulting behavior of the disc as it undergoes a limit cycle, making repeated transitions between a cool quiescent state and a hot, viscous outburst state. With various modifications, the DIM has been successful in both explaining the outbursts of dwarf novae and providing a basic framework for understanding the outbursts of their more massive analogs, the XRBs (*1*).

SS Cygni is the brightest and best-studied dwarf nova, with an optical light curve containing close to 500,000 observations stretching back to its discovery in 1896. It shows repeated outbursts with a mean recurrence time of 49 ± 15 days (*2*). For a distance of ~100 pc, the outburst properties can be well reproduced by the DIM when including the effects of a truncated inner disc and small variations in the mass transfer rate from the secondary (*3*). However, the optical parallax measured by the Hubble Space Telescope (HST) (*4*–*6*) places the source at a distance of 159 ± 12 pc, implying that it has the highest absolute visual magnitude of any dwarf nova (*7*). The mass accretion rate required during outburst to generate this optical luminosity is then too high to be compatible with the DIM, because the mean mass transfer rate becomes high enough that the disc should be persistently in the hot, ionized, stable state. SS Cygni should then appear as a nova-like CV with no outbursts. At a distance of 159 pc, the difference in behavior between SS Cygni and the more stable nova-like CVs with similar binary parameters cannot then be ascribed to a difference in the mean mass transfer rate (*8*). This would contradict not only the key prediction of the DIM, but our entire understanding of accretion discs in CVs (*9*) and other accreting systems (*10*, *11*). The only possible explanation would be an enhancement in mass transfer rate during outburst (*12*), but the required enhancement factor of 150 is implausibly high (*13*).

Because SS Cygni is known to emit radio emission during outbursts (*14*), we used very long

[1]International Centre for Radio Astronomy Research, Curtin University, G.P.O. Box U1987, Perth, WA 6845, Australia. [2]Department of Physics, University of Alberta, CCIS 4-183 Edmonton, AB T6G 2E1, Canada. [3]Department of Astronomy, University of Virginia, P.O. Box 400325, Charlottesville, VA 22904, USA. [4]School of Physics and Astronomy, University of Southampton, Highfield, Southampton SO17 1BJ, UK. [5]Department of Astrophysics/IMAPP, Radboud University Nijmegen, P.O. Box 9010, 6500 GL Nijmegen, Netherlands. [6]American Association of Variable Star Observers, 49 Bay State Road, Cambridge, MA 02138, USA.

*Corresponding author. E-mail: james.miller-jones@curtin.edu.au

Table 1. Fitted astrometric parameters for SS Cygni. Uncertainties are 1σ.

Parameter	Fitted value
Right ascension α_0 (J2000)	21:42:42.923121 ± 0.000006
Declination δ_0 (J2000)	43:35:10.25301 ± 0.00007
Proper motion in right ascension ($\mu_\alpha \cos\delta$; mas year^{-1})	112.42 ± 0.07
Proper motion in declination (μ_δ; mas year^{-1})	33.38 ± 0.07
Parallax (mas)	8.80 ± 0.12
Distance (pc)	114 ± 2
Reference epoch (MJD)	55,769.0